Mechanics & Industry **19**, 311 (2018)
© AFM, EDP Sciences 2018
https://doi.org/10.1051/meca/2018028

Mechanics & Industry

Available online at:
www.mechanics-industry.org

Regular Article

Real-time simulation test-bed for an industrial gas turbine engine's controller

Morteza Montazeri-Gh, Seyed Alireza Miran Fashandi*, and Soroush Abyaneh

Systems Simulation and Control Laboratory, School of Mechanical Engineering, Iran University of Science and Technology, Tehran, Iran

Received: 20 August 2017 / Accepted: 18 May 2018

Abstract. A hardware-in-the-loop (HIL) test for a control unit of an industrial gas turbine engine is performed to evaluate the designed controller. Although the dynamic performance of the studied gas turbine is strictly related to the variable inlet guide vain (VIGV) position, one of the main challenges is to develop an engine model considering VIGV variations. The model should also be capable of real time simulation. Accordingly, the gas turbine is numerically modeled using bond graph concepts. To demonstrate the operational reliability of the engine's control strategy, the control algorithm is implemented on an industrial hardware as an embedded system. This is then put into a HIL test along with the engine model. The actual component (controller) and the virtual engine model are the hardware and software parts of the HIL test, respectively. In this experiment, the interaction between the real part and the rest of the system is compared with that of the completely numerical model in which the controller is a simulated software-based model as is the engine itself. Finally, the results indicate that the physical constraints of the engine are successfully satisfied through the implementation of control algorithms on the utilized hardware.

Keywords: Bond graph / industrial gas turbine engine / electronic control system / hardware-in-the-loop simulation

1 Introduction

A key factor in designing complex systems and structures is the ability to test every subsystem in each design stage to ensure a convergent design strategy. In this regard, various theoretical and experimental procedures have been considered. The hardware-in-the-loop (HIL) simulation has proven to be one of most efficient method for testing complicated and costly systems. HIL simulation has been used extensively in a variety of fields for real-time testing and development of interconnected physical components of a system replaced virtually by computer models. Interaction between hardware and software during the test is accomplished via electric signals transferred by data acquisition cards. Consequently, HIL simulation is widely used in numerous applied fields and industries. Using this approach, it is possible to test the performance of real mechanical parts of a system along with software-based simulated models of other parts in real time [1,2].

One of the requirements of HIL test is designing and constructing a test-system so as to experiment with different parts of a complex system in accordance with the defined rules. Furthermore, to make HIL more cost-effective, the main system in which we are interested to design should be numerically modeled. These hardware and software models are then put into a loop together for experiment.

Hanselman [3] benefited from HIL simulation in the control development of electronic control units (ECUs) used in engines, vehicles and other components. Cao et al. [4] verified the validity of their control scheme based on adaptive network-based fuzzy inference engine using HIL test. Gans et al. [5] presented another HIL simulation to control unmanned vehicles. In that study, a real camera captured pictures of a virtual 3D environment which would later be used in the control system. Aerospace is another field where HIL has progressively been utilized as Maclay [6] enumerated several examples. Canadian Space Agency successfully applied HIL in meticulously tuning controllers used in the International Space Station. A non-gravity environment for the controllers was simulated using HIL. The simulation results were acceptable compared to practical tests [7]. In the gas turbine industry, HIL applications are innumerable, specifically for designing, testing and performance verification of the gas turbine engine's ECU or fuel control unit (FCU). HIL simulation

* e-mail: alirezamiran@mecheng.iust.ac.ir; s.alireza.miran@gmail.com

studies have been reported for rapid prototyping of ECU of turbofan engines [8,9] and turbojet engines [10,11]. An HIL simulation is reported by Montazeri-Gh et al. [12] for ECU performance verification of a turbo-shaft engine. Another HIL simulation is presented by Montazeri-Gh et al. [13] for testing a fuel control unit of a jet engine.

Despite numerous reports on HIL simulation of a gas turbine engine's ECU or FCU, there has not been any publication regarding HIL simulation of a two-shaft industrial gas turbine engine modeled using bond graph methodology. As an example of bond graph power in modeling gas turbine engines, Novinzadeh et al. used this method to simulate an ideal turbocharger [14]. Montazeri et al. [15] showed how bond graph approach can be utilized for modeling the cold start phase of a microjet engine.

Moreover, Krikelis and Papadakis [16] modeled a simple cycle of the single-shaft gas turbine using bond graph model. By linearization of the model around an operation point, they designed a PI controller for it. In addition, they utilized several parameters including the pressure, temperature and torque as the effort variables, as well as the mass flow rate and engine speed (rpm) as the flow variables.

Sanei et al. [17] considered the effects of kinetic energy and momentum (in the convergent-divergent nozzles with supersonic fluid flows) using the pseudo-bond graph approach.

Uddin and Gravdahl [18] developed the bond graph model of a radial compressor system, and complemented it with a control system. They also developed certain methods to prevent the surge in the compressor. Montazeri and Miran-F [19] presented the bond graph approach application for modeling the industrial gas turbine engine. The bond graph model developed in that study was applicable to the real time implementation. A more comprehensive study using bond graph was later accompanied by the modeling and simulation of the propulsion system of a two-shaft gas turbine including a plate-type clutch [20] as well as another related study on JetQuard aerial robot [21]. This was similar to other gas turbine nonlinear models [22–24] involving thermodynamics equations as well as compressor and turbine performance maps. Therefore, the bond graph model seems appropriate for controlling purposes during an HIL simulation as is the case in present study.

In this article, the designed control system of a two-shaft industrial gas turbine engine, along with the engine's ECU (as a physical model), is tested in an HIL simulation. The utilized ECU is an electronic hardware called PC/104, which is an embedded system on which the control algorithm has been implemented via C++ programming language. The engine model is actually a bond graph model simulated on a personal computer using 20SIM and Matlab/Simulink. The interface between hardware and software subsystems is realized by an I/O data acquisition card.

To examine the performance of ECU to ensure the accuracy of its operation, the results are compared with the simulation results of the same system in which the ECU is numerically simulated. Such simulation is called software-in-the-loop (SIL) simulation.

2 System description

The schematic of the system as well as the interaction of different parts in HIL and SIL test is shown in Figure 1a–c. It is a feedback control system composed of two main subsystems including the plant and the controller. Only the plant is simulated numerically, while the ECU is a hardware within the HIL simulation. The plant, a two-shaft industrial engine (SGT600) [25] with two outputs and two inputs, is a gas turbine engine model. The engine specifications at the design point are given in Table 1 [25]. The plant's inputs are the required fuel flow rate to the combustion chamber of the gas turbine engine and the required variable inlet guide vain (VIGV) position. The engine outputs are the angular velocities of the power gas turbine engine shaft (N_{PT}) and the gas generator shaft (N_{GG}). The gas turbine engine has two bleed valves which are considered to be closed during the engine modeling process at a specific state in this article. This state is demonstrated in Figure 2, indicating that their effect is negligible. The plant controller, known as the ECU, calculates the appropriate fuel flow rate and the required VIGV at every moment based on its inputs, and accordingly generates control signals towards the plant. VIGV position is a function of N_{GG} and thus, the effects of VIGV variations are considered in the engine's performance maps. The ECU has three inputs, two of which are the angular velocities of the engine that are fed back to the ECU, and a reference angular velocity which is set by the user. RRV is a preferred angular velocity with which the power turbine shaft rotates. The outputs are the fuel flow rate and VIGV, as stated previously.

2.1 Plant

The engine components [19] (compressor, combustor and turbine) are simulated according to the bond graph theory. Every component is assumed to be an energy field interacting with other components, i.e. mass, energy and work are permanently exchanged in all components. The gas turbine engine is considered to be a thermo-fluid system, and the effort and flow variables are selected as introduced by Karnopp [19,26]. According to this variable selection, the pseudo-bond graph is advantageous over the true bond graph. The effort and flow variables of the compressor and turbine are torque and engine speed. Mass flow rate and pressure are the flow and effort variables in one pseudo-bond while energy flow and temperature are the variables for another pseudo-bond. In order to obtain a gas turbine model using the bond graph theory, it is necessary to take the following criteria into consideration:

- model simplicity;
- inclusion of the control model in engine model to observe the physical limitations of the engine;
- dynamic operation and steady state performance predictability;
- considering the change in the composition of working medium.

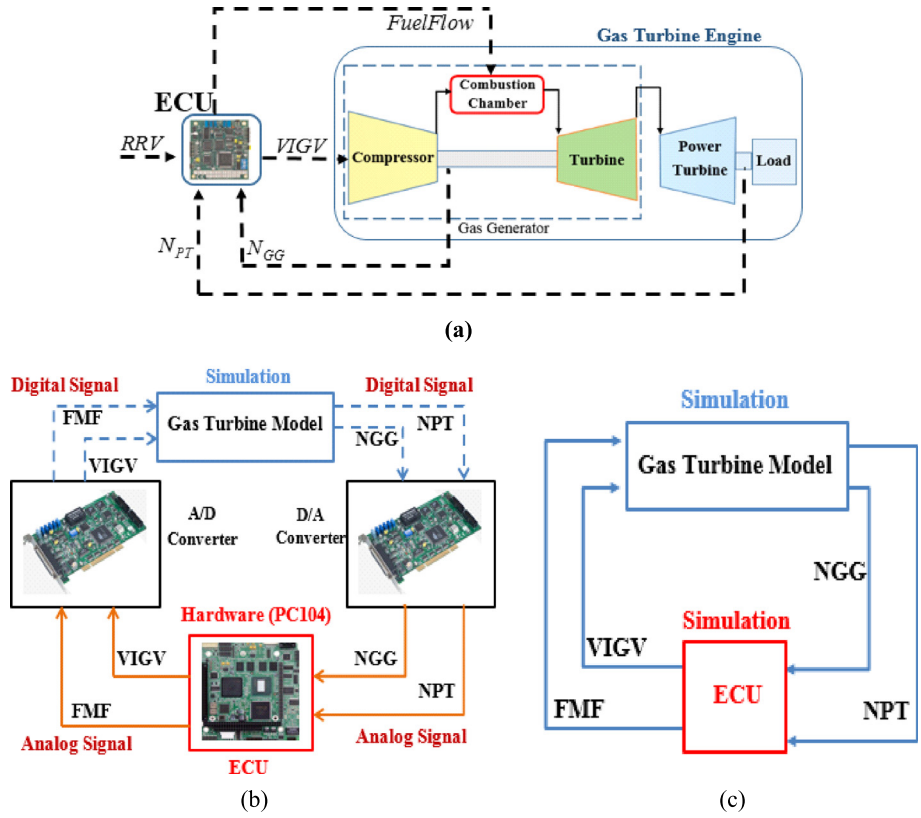

Fig. 1. Schematics of (a) complete system, (b) HIL test, and (c) SIL test

Generally, two different approaches are employed to develop the model of compressor or turbine. One is based on the turbo-machinery fundamental equations. Such approach requires not only a thorough understanding of the machine, but also considering some simplifying assumption that may lead to limited accuracy.

The other approach requires taking the state performance maps into account. These maps contain valuable performance information of the machine over a large operational range. Also, no mass and energy accumulation within the compressor and turbine models are considered (quasi-steady assumption). As a result, the performance map for steady state condition is valid even during transient operation.

Finally, to show the accuracy of utilized bond graph model, the reader is referred to references [19,20] where it was used for a gas turbine and good agreement was obtained.

2.1.1 Compressor model equations

The isentropic efficiency and corrected mass flow rate of the compressor vary in accordance with three compressor parameters: inlet guide vanes, pressure ratio and corrected rotor speed [19,22]. These are described as

$$\begin{aligned} \Gamma_{\mathrm{C}} &= f_1(\pi_{\mathrm{C}}, N_{\mathrm{C,cor}}, \theta_{\mathrm{VIGV}}), \\ \eta_{\mathrm{is},C} &= f_2(\pi_{\mathrm{C}}, N_{\mathrm{C,cor}}, \theta_{\mathrm{VIGV}}), \end{aligned} \tag{1}$$

$$\Gamma_{\mathrm{C}} = \frac{\dot{m}_C\sqrt{\theta}}{\delta}, \quad N_{\mathrm{C,cor}} = \frac{N_{\mathrm{GG}}}{\sqrt{\theta}}, \quad \pi_{\mathrm{C}} = \frac{P_{\mathrm{out}}}{P_{\mathrm{in}}}, \tag{2}$$

$$M_C = \frac{30}{\pi}\left[\frac{\dot{m}_C(h_{\mathrm{is,out}} - h_{\mathrm{in}})}{\eta_{\mathrm{is,C}} N}\right],$$

$$T_{\mathrm{out}} - T_{\mathrm{in}} = \frac{T_{\mathrm{in}}}{\eta_C}\left[\left(\frac{P_{\mathrm{out}}}{P_{\mathrm{in}}}\right)^{\frac{\gamma-1}{\gamma}} - 1\right], \tag{3}$$

$$\dot{E}_{\mathrm{in}} = \dot{m}_C h_{\mathrm{in,C}}, \tag{4}$$

where Γ_{C}, π_{C}, $N_{\mathrm{C,cor}}$, $\eta_{\mathrm{is,C}}$, M_{C} and $\dot{m}_C$ are, respectively, the corrected mass flow rate, pressure ratio, corrected rotor speed, isentropic efficiency, torque and air mass flow rate of the compressor. Moreover, N_{GG} is the gas generator speed, P_{out} is the outlet pressure, (P_{in}, h_{in}) are the inlet pressure and enthalpies, $h_{\mathrm{is,out}}$ is the outlet isentropic enthalpy, (T_{out}, T_{in}) are the outlet and inlet temperatures and γ is the specific heat ratio. Finally, E being the internal energy, ($\dot{E}_{\mathrm{in}}$, $\dot{E}_{\mathrm{out}}$) describe the energy flow in and out of the compressor.

By definition, the dimensionless pressure and temperature are defined as $\delta = P_{\mathrm{in}}/P_{\mathrm{ref}}$ and $\theta = T_{\mathrm{in}}/T_{\mathrm{ref}}$, respectively, where P_{ref} and T_{ref} represent the standard pressure and temperature (ISA).

Table 1. Design point characteristics of the examined gas turbine engine [19,25].

Quantity	Value
Power, MW	24.77
Exhaust gas temperature, °C	543
Exhaust gas flow, kg/s	80.4
GG turbine speed, rpm	9705
Compressor pressure ratio	14
Power turbine speed, rpm	7700
Thermal efficiency, %	34.2

2.1.2 Combustion chamber model equations

For the combustion chamber, the following assumptions are considered: volume of the chamber is constant and physical and chemical properties of fuel and air mixture are the same throughout the chamber [19,22]. Based on the conservation laws of mass (Eq. (5)) and energy (Eq. (6)), the combustion chamber equations are expressed as

$$\frac{\mathrm{d}m}{\mathrm{d}t} = \dot{m}_{\mathrm{in}} - \dot{m}_{\mathrm{out}} + \dot{m}_{\mathrm{f}}, \tag{5}$$

$$\frac{dU}{\mathrm{d}t} = \dot{m}_{\mathrm{in}} h_{\mathrm{in}} - \dot{m}_{\mathrm{out}} h_{\mathrm{out}} + \dot{m}_{\mathrm{f}}(h_{\mathrm{f}} + \mathrm{LHV}\eta_{\mathrm{cc}}), \tag{6}$$

where LHV is the heat value of fuel, m_{f} is the fuel mass, m_{air} is the air mass and η_{cc} is the combustor efficiency. By differentiation the above equations, one can obtain

$$\frac{\mathrm{d}U}{\mathrm{d}t} = C_v T \frac{\mathrm{d}m}{\mathrm{d}t} + C_v m \frac{\mathrm{d}T}{\mathrm{d}t}, \tag{7}$$

where C_{v} is the specific heat at constant volume. Setting equation (6) equal to equation (7), and then using the ideal gas law, the temperature and pressure of chamber exhaust are described as

See equation (8) and (9) below page

Finally, the fuel-to-air ratio is expressed by

$$f = \frac{m_f}{m_{\mathrm{air}}} = \frac{m_f}{m - m_f}. \tag{10}$$

2.1.3 Gas generator turbine model equations

In a similar manner, the isentropic efficiency and corrected mass flow rate of the turbine are dependent on two turbine parameters: expansion ratio and corrected rotor speed [19,22], written in the form

$$\Gamma_{\mathrm{T}} = g_1(\pi_{\mathrm{T}}, N_{\mathrm{T,cor}}), \quad \eta_{\mathrm{is,T}} = g_2(\pi_{\mathrm{T}}, N_{\mathrm{T,cor}}), \tag{11}$$

$$\Gamma_{\mathrm{T}} = \frac{\dot{m}_{\mathrm{c}}\sqrt{\theta}}{\delta}, \quad N_{\mathrm{T,cor}} = \frac{N_{\mathrm{GG}}}{\sqrt{\theta}}, \quad \pi_{\mathrm{T}} = \frac{P_{\mathrm{in}}}{P_{\mathrm{out}}}, \tag{12}$$

$$M_T = \frac{30}{\pi}\left[\frac{\eta_T \dot{m}_T (h_u - h_{\mathrm{d,is}})}{N}\right], \tag{13}$$

$$\dot{E}_{\mathrm{in}} = \dot{m}_T h_{\mathrm{u,T}}, \tag{14}$$

$$\dot{E}_{\mathrm{out}} = \dot{m}_T\left[h_{\mathrm{u,T}} + \frac{(h_u - h_{\mathrm{d,is}})}{\eta_T}\right], \tag{15}$$

where g represents a function, i.e. the corrected mass flow rate (Γ_{T}) and isentropic efficiency ($\eta_{\mathrm{is,T}}$) are both functions of expansion ratio and corrected rotor speed.

2.1.4 Plenum equations

The plenum is taken as an isentropic passage in which energy and flow speed are not significant and thus are neglected. The governing equations to obtain the plenum pressure in addition to the temperature variation caused by the mass accumulation can be written as

$$\begin{aligned} V_p \frac{\mathrm{d}\rho_{\mathrm{out}}}{\mathrm{d}t} &= \frac{V_P}{\delta R T_{\mathrm{out}}} \frac{\mathrm{d}p_{\mathrm{out}}}{\mathrm{d}t} = \dot{m}_{\mathrm{in}} - \dot{m}_{\mathrm{out}} \\ \frac{\mathrm{d}T_{\mathrm{out}}}{\mathrm{d}t} &= \frac{\delta}{\rho c_p V_p}\left[(c_p T \dot{m})_{\mathrm{in}} - (c_p T \dot{m})_{\mathrm{out}}\right] + \frac{T_{\mathrm{out}}}{\rho V_p}(\dot{m}_{\mathrm{out}} \\ &\quad - \dot{m}_{\mathrm{in}}), \end{aligned} \tag{16}$$

where V_{p} is the plenum volume. Moreover, c_{p} and ρ are the constant pressure heat capacity, respectively. δ can be estimated by the specific heat ratio [19,22].

2.1.5 Gas turbine shaft model equations

The gas generator shaft acceleration is due to the difference between the turbine output shaft power and the input power to the compressor. It should be noted that the variations in the load applied to the power turbine shaft causes changes in the power turbine speed. This leads to the acceleration of the connector shaft between the power turbine and generator (load). Accordingly, the gas generator shaft along with the power turbine shaft can

$$\frac{\mathrm{d}T}{\mathrm{d}t} = \frac{\dot{m}_{\mathrm{in}} h_{\mathrm{in}} \dot{m}_{\mathrm{out}} h_{\mathrm{out}} + \dot{m}_f(h_f + \mathrm{LHV}\eta_{\mathrm{cc}}) C_{\mathrm{v}} T(\dot{m}_{\mathrm{in}} \dot{m}_{\mathrm{out}} + \dot{m}_f)}{C_v m}, \tag{8}$$

$$\frac{P}{m}(\dot{m}_{\mathrm{in}} \dot{m}_{\mathrm{out}} + \dot{m}_f) + \frac{P}{T}\left[\frac{\dot{m}_{\mathrm{in}} h_{\mathrm{in}} \dot{m}_{\mathrm{out}} h_{\mathrm{out}} + \dot{m}_f(h_f + \mathrm{LHV}\eta_{\mathrm{cc}}) C_{\mathrm{v}} T(\dot{m}_{\mathrm{in}} \dot{m}_{\mathrm{out}} + \dot{m}_{\mathrm{f}})}{C_v m}\right] = \frac{\mathrm{d}P}{\mathrm{d}t}. \tag{9}$$

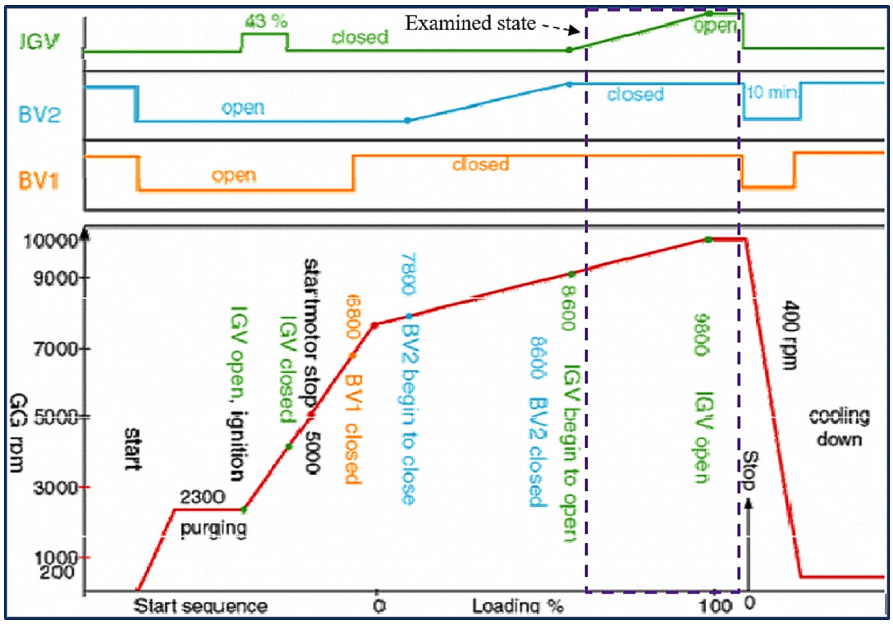

Fig. 2. Schematics of the bleed valve (BV) and IGV functions of the gas turbine [29].

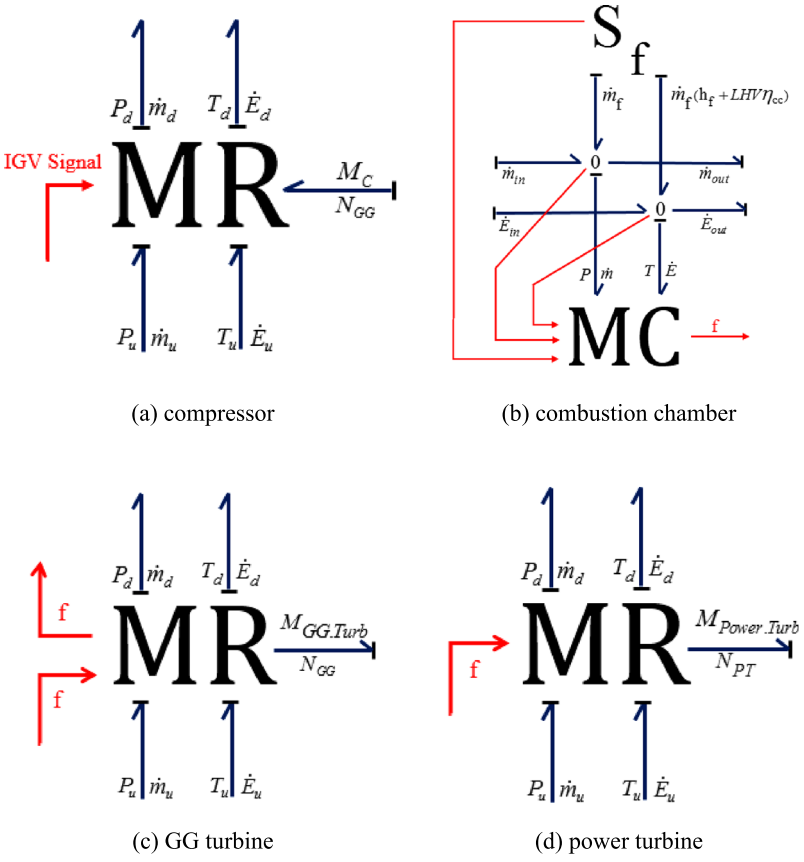

(a) compressor (b) combustion chamber

(c) GG turbine (d) power turbine

Fig. 3. Pseudo-bond graph models of the gas turbine components [19].

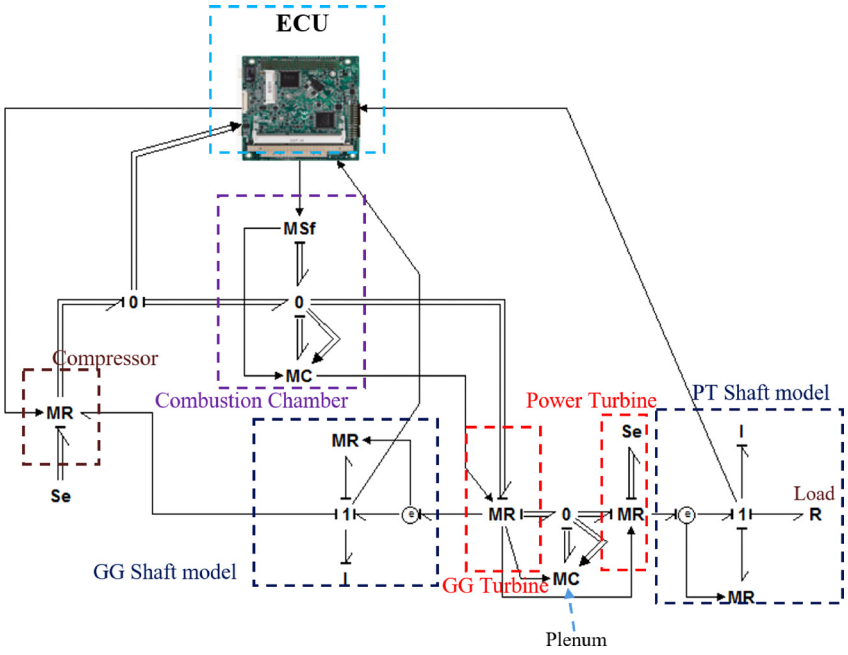

Fig. 4. Complete bond graph model of the engine.

be described using mathematical relations as in

$$\begin{aligned} M_{\text{fric,GG}} &= \eta_{\text{mech,GG}} M_{\text{GG.Turb}} \\ M_{\text{fric,PT}} &= \eta_{\text{mech,PT}} M_{\text{Power.Turb}} \end{aligned}, \tag{17}$$

$$\frac{\mathrm{d}N_{\text{GG}}}{\mathrm{d}t} = \frac{30}{\pi I_{\text{GG}}} (M_{\text{GG.Turb}} - M_C - M_{\text{fric,GG}}), \tag{18}$$

$$\frac{\mathrm{d}N_{\text{PT}}}{\mathrm{d}t} = \frac{30}{\pi I_{\text{PT}}} (M_{\text{Power.Turb}} - M_L - M_{\text{fric,PT}}), \tag{19}$$

where $\eta_{\text{mech,GG}}$ and $\eta_{\text{mech,PT}}$ represent the mechanical efficiency of, respectively, the gas generator and power turbine. In addition, ($M_{\text{fric,GG}}$, $M_{\text{GG.Turb}}$) and ($M_{\text{fric,PT}}$, $M_{\text{Power.Turb}}$) are the friction and turbine torque of, respectively, the gas generator and power turbine. Furthermore, M_{L} signify the consumed torque as a result of applied load on the power turbine shaft.

Figure 3 shows the component models. The compressor, combustion chamber and turbine are modeled via modulated energy fields (MR, MC and MR). IGV and fuel-to-air-ratio (f) signals are transferred to the compressor and turbine by informative bonds. When the bond graphs of all sub-models are coupled, a complete gas turbine engine dynamic model would be constructed, as shown in Figure 4.

2.2 ECU

ECU is the master mind of the system. It computes the necessary amount of required fuel as well as the appropriate IGV position for the engine to provide a satisfactorily operation and ensure a safe performance. The fuel control algorithm is based on the Min-Max control strategy. The IGV control algorithm is a function of the angular velocity of the gas generator shaft. Upon designing the control algorithm in 20SIM [27] and Matlab/Simulink, its precise and non-destructive performance is tested by the computer. As in every gas turbine engine design and construction process, ECU eventually needs to be implemented on a hardware. In this study, a microprocessor called PC/104 has been used. In addition, the Min-Max control strategy for fuel controlling along with the IGV control function are implemented using C++ language. The models of plant [19] and ECU [12,28] as well as PC/104 specifications used for this study were discussed in detail in previous studies.

The Min-Max controller is composed of five transient control loops and a single steady state control loop, as depicted in Figure 5. In each loop, the required fuel to fulfill the needs of that loop is calculated. Next, a Min-Max algorithm is used for fuel selection throughout the engine operation. This algorithm is written as [12]

$$F_{\text{trans}} = \text{Max}\left[F_{\text{dec}}, \text{Min}\left(F_{\text{acc}}, F_{\text{NGG}_{\text{max}}}, F_{\text{NPT}_{\text{max}}}, F_{\text{NPT}_{\text{requried}}}\right)\right], \tag{20}$$

$$F_{\text{total}} = F_{\text{trans}} + F_{\text{steady}}. \tag{21}$$

The description of each parameter is presented in Table 2.

In order to assess the performance of this controller, an input load is applied to the engine, as demonstrated in Figure 6. As shown in Figures 7–9, N_{GG} (NGG), N_{PT} (NPT) and their rate of change have been kept within allowable limits. Also, N_{PT} approximately remains at its desired set value.

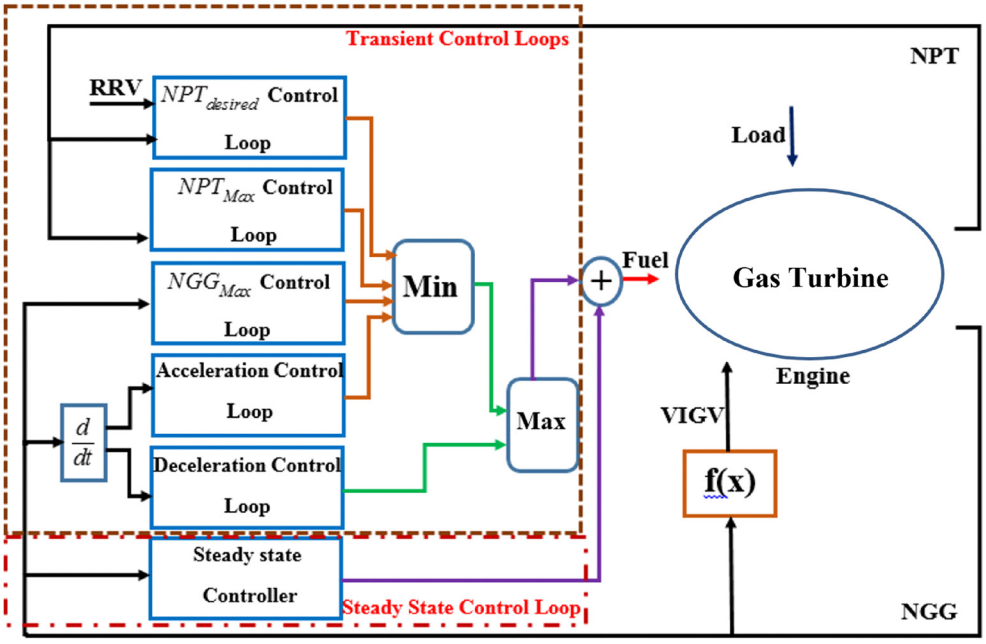

Fig. 5. Controller structure [19].

Table 2. Parameter description of equations (20)–(21).

Component	Specification
F_{dec}	Computed fuel by the maximum deceleration control loop
F_{acc}	Computed fuel by the maximum acceleration control loop
$F_{\text{NGG}_{\text{max}}}$	Computed fuel by the maximum NGG control loop
$F_{\text{NPT}_{\text{max}}}$	Computed fuel by the maximum NPT control loop
$F_{\text{NPT}_{\text{requried}}}$	Computed fuel by the required NPT control loop
F_{trans}	Required fuel for transient condition
F_{steady}	Required fuel for steady state condition
F_{total}	Final required fuel is then applied to the engine

3 HIL setup

In order to evaluate the performance accuracy of the ECU and its proper implementation, a real time HIL simulation test-bed is prepared as displayed in Figure 10.

The gas turbine engine model, created using 20SIM and Simulink/Matlab, is loaded on a PC labeled "1" in the figure. The control algorithm is embedded on VDX6354 PC/104 (labeled "2") as the ECU, via a C++ code.

The VDX-6354 family of controllers is designed as a plug-in replacement to support legacy software and help extend the existing product life cycle without heavy re-engineering. VDX-6354 is suitable for a broad range of data-acquisition tasks, industrial automation, process control, automotive controller, AVL, intelligent vehicle management device, medical device, human machine interface, robotics, machinery control, in addition to applications that require small footprint, low-power and low-cost hardware with open industry standard such as PC/104. Transmission of signals from software-based engine model to the hardware-based ECU model and vice versa is rendered by a data acquisition card, Advantech PCL-812PG I/O (labeled "3"). PC/104 VGA output is connected to a monitor (labeled "4") to enable the user to edit the C++ code of the control algorithm.

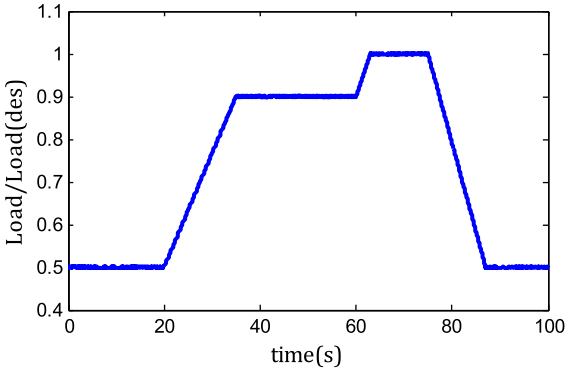

Fig. 6. Load input to the gas turbine model.

4 HIL results

To conduct an HIL simulation, an input load is designated by the user. In this study, the load is selected to be a combination of some ramp and step inputs, as indicated in Figure 11. The load starts from its minimum value and remains constant for about 20 s, then increases to its maximum load value in two consecutive steps after 60 s and finally returns to its initial value. This should be considered

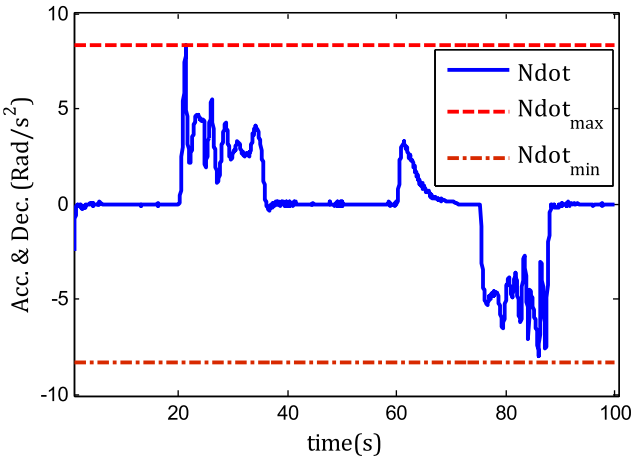

Fig. 7. Variation of the gas generator turbine shaft acceleration.

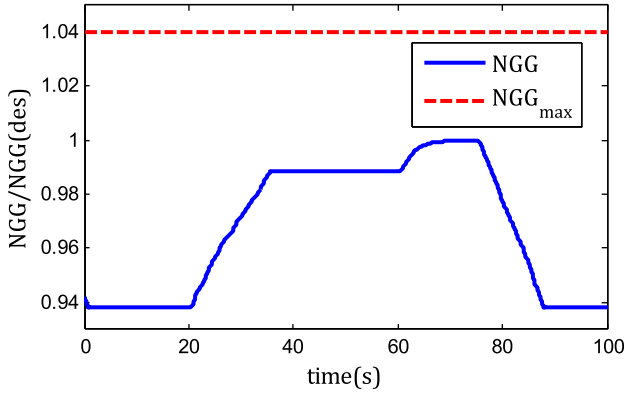

Fig. 8. Variation of the gas generator shaft speed.

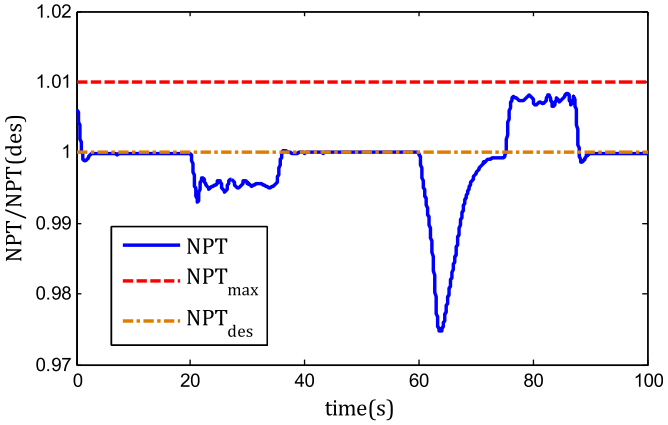

Fig. 9. Variation of the power turbine shaft speed.

as the worst-case scenario of load since it involves acceleration along with deceleration for a very short period of time with a relatively steep trend. Should the assumed control strategies keep the system operating in the desired range, they will most likely do for other load function.

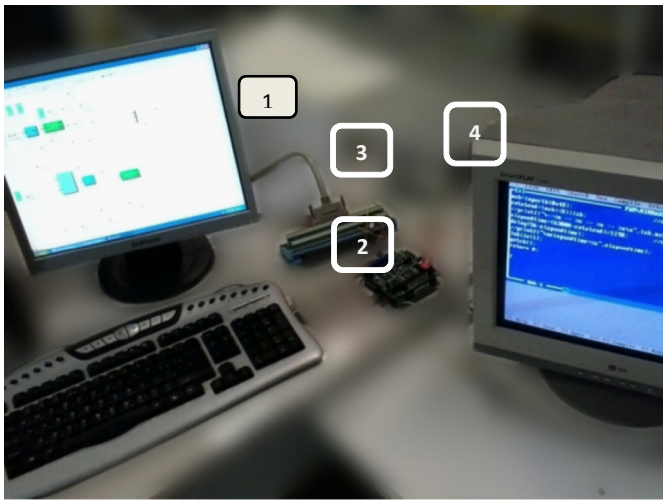

Fig. 10. HIL simulation of the test-bed.

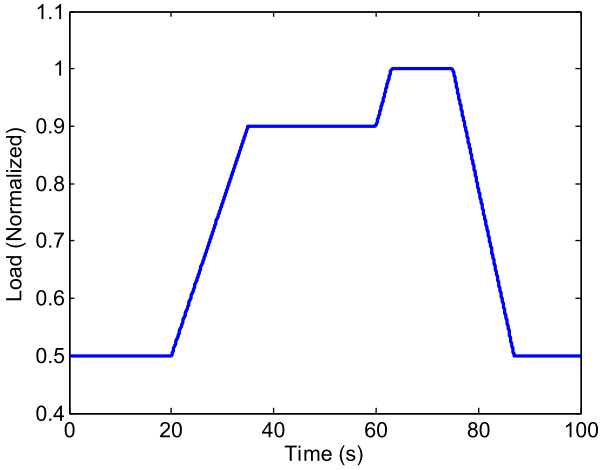

Fig. 11. Applied load to the HIL simulation.

The HIL simulation results are compared with those of SIL simulation when subjected to the same load.

Figure 12 shows the result of N_{GG} in SIL and HIL simulations. It shows that N_{PT} closely follows the load trend, and a rise or fall in the load will cause the same effect in N_{GG} plot. In addition, N_{GG} changes based on the change in load with virtually no observed lag for both case of SIL and HIL simulations. This indicates that the control strategies on N_{GG} are satisfactory and the implementation is properly carried out for HIL test.

Normalized N_{PT} from HIL and SIL simulations are illustrated in Figure 13. NPT tends to remain at its desired set value (RRV). However, the ECU designates a new fuel demand for the engine when a sudden change in the load occurs. As a result, some oscillations occur in N_{PT} until it reaches its defined value. Fuel mass flow rate for HIL simulation and SIL tests are demonstrated in Figure 14. Upon load deviation, the fuel flow to the engine is decreased and vice versa, as indicated by the simulation results.

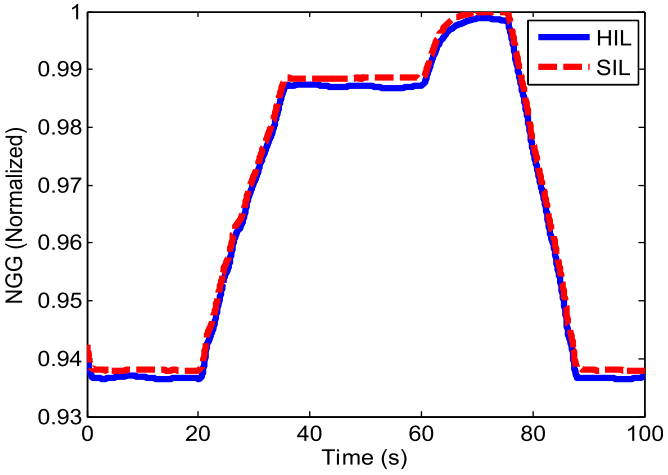

Fig. 12. HIL and SIL simulation results for N_{GG} signal.

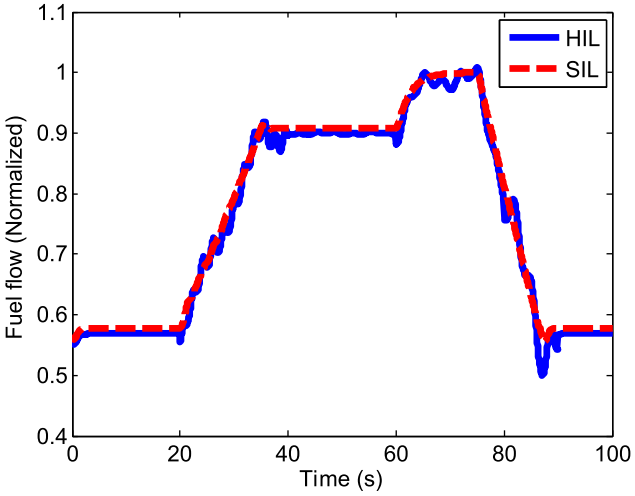

Fig. 14. HIL and SIL simulation results for fuel flow signal.

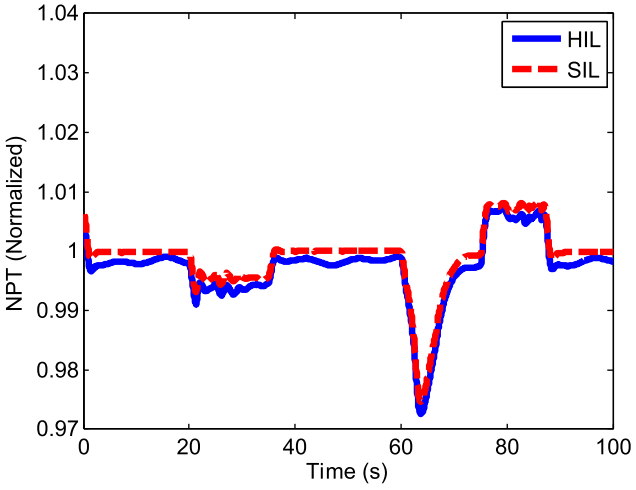

Fig. 13. HIL and SIL simulation results for N_{PT} signal.

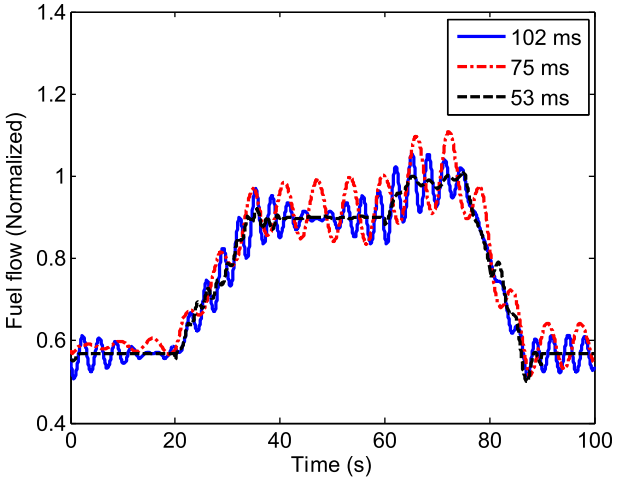

Fig. 15. Fuel flow signal for three HIL simulations with different sampling times.

Sampling time plays a key role in HIL simulations for the physical part of the test system, i.e. PC/104 microprocessor. Choosing an appropriate sampling time for every HIL simulation is an essential part of the test. Figure 15 shows the effect of different sampling times (53 ms, 75 ms and 102 ms) for the same HIL simulation described in the previous section.

As can be observed, the higher the sampling time, the more oscillatory the test results are. Nevertheless, relative accuracy is reached for the sampling time of about 53 ms. To put it more accurately, sampling time greatly affects the results stability. By choosing a small sampling time, the simulation time for a sampled data may not match the require time and addition of new sampled data may end in results divergence. A similar discussion can be made on long simulation time where the simulation may be left with no data input for a period, which may lead to instability. There are recommendations for choosing sampling time, but the best one is obtained through trial and error, as carried out in this study.

5 conclusion

In this article, an industrial gas turbine engine with two shafts and variable IGVs was studied. The VIGV position and the engine inlet fuel were considered as the controlling parameters of the engine. Since the performance characteristic of the engine is highly dependent on VIGVs, a modeling procedure was chosen to take this effect into account (bond graph modeling). The ECU of this gas turbine engine provides the required fuel flow as well as VIGV operational position. To evaluate the accuracy of the designed control system, the control strategy was implemented on an electronic hardware and tested in real time via some comprehensive HIL simulations. Every physical constraint of the engine is satisfied by fuel and VIGV position, indicating the successful implementation of the control algorithm on the PC/104 hardware. Changes in bleed valves can be the subject and future studies, while HIL test can be carried out at lower speed and in the start-up phase of gas turbine. A small rounding of the load ramp

corner is also necessary to obtain better results. Finally, a more advanced control system such as model predictive control can be used to perform HIL test.

Nomenclature

acc	Acceleration
BG	Bond graph
c_p	Constant pressure specific heat
c_v	Constant volume specific heat
CAMF	Compressor air mass flow
CPR	Compressor pressure ratio
dec	Deceleration
e	Effort sensor
$\dot{E}$	Energy flow
ECU	Electronic control unit
EGT	Exhaust gas temperature
f	Fuel to air ratio
FCU	Fuel control unit
FMF	Fuel mass flow
h	Enthalpy
HIL	Hardware-in-the-loop
M M	Torque
m	Mass
$\dot{m}$	Mass flow rate
Max	Maximum
Min	Minimum
N	Rotational speed
N_{GG}, NGG	Gas generator speed
N_{PT}, NPT	Power turbine speed
P	Pressure
R	Universal gas constant
RRV	Desired power turbine speed
SIL	Software-in-the-loop
T	Temperature
VIGV	Variable inlet guide vane
Γ	Corrected mass flow rate
γ	Specific heat ratio
δ	Dimensionless pressure
η	Efficiency
θ	Dimensionless temperature
π	Pressure ratio

Subscripts

C	Compressor
CC	Combustion chamber
d	Downstream
fric	Friction
GG	Gas generator
in	Inlet
is	Isentropic
L	Load
mech	Mechanical
out	Outlet
PT, Power.Turb	Power turbine
ref	Standard value (of pressure or temperature)
T, Turb	Turbine
trans	Transient
u	Upstream

References

[1] H.K. Fathy, Review of hardware-in-the-loop simulation and its prospect in the automotive area, Society of Photo-optical Instrumentation Engineers, Proc. SPIE 6228 (2006)

[2] R. Isermann, J. Schaffnit, S. Sinsel, Hardware-in-the-loop simulation for the design and testing of engine-control systems, Control Eng. Pract. 7 (1999) 643–653

[3] H. Hanselman, Hardware-in-the-loop simulation testing and its integration into a CACSD toolset, in: The IEEE International Symposium on Computer-Aided Control System Design, Dearborn, Michigan, USA, 1996, pp. 152–156

[4] Y. Cao, W. Teng, H. Zhang, Hardware-in-the-loop simulation for engine idle speed control based on Adaptive Neural Fuzzy Inference Engine, IEEE, 2008

[5] N.R. Gans, W.E. Dixon, R. Lind, A. Kurdila, A hardware in the loop simulation platform for vision-based control of unmanned air vehicles, Mechatronics 19 (2009) 1043–1056

[6] D. Maclay, Si mulation gets into the loop, IEE Review (1997) 109–112

[7] J.C. Piedboeuf, M. Doyon, R. L'Archeveque, E. Martin, Simulation environments for space robot design and verification, in: Advanced Space Technologies for Robotics and Automation, Noordwijk, The Netherlands, 2000

[8] H. Wang, Y. Guo, J. Lu, Design and validation of aeroengine control system with non-fully recovering LQG/LTR method, in: Second International Conference on Innovative Computing, Information and Control, ICICIC0, 2007, Art. No. 4428111, 2008

[9] L. Jun, G. Ying-Qing, W. Hai-Quan, Rapid prototyping real-time simulation platform for digital electronic engine control, in: Second International Symposium on Systems and Control in Aerospace and Astronautics, ISSCAA, 2008, Art. No. 4776230, 2008

[10] M. Montazeri-Gh, M. Nasiri, S. Jafari, Real-time multi-rate HIL simulation platform for evaluation of a jet engine fuel controller, Simul. Model. Pract. Theory 19 (2011) 996–1006

[11] A. Watanabe, S.M. Ölçmen, R.P. Leland, K.W. Whitaker, L.C. Trevino, C. Nott, Soft computing applications on a SR-30 turbojet engine, Fuzzy Sets Syst. 157 (2006) 3007–3024

[12] M. Montazeri-Gh, S. Abyaneh, S. kajemnejad, Hardware-in-the-loop simulation of two-shaft gas turbine engine's electronic control unit, Proc. Inst. Mech. Eng. Part I: J. Syst. Control Eng. 230 (2016) 512–521

[13] M. Montazeri-Gh, M. Nasiri, M. Rajabi, M. Jamshidfard, Actuator-based hardware-in-the-loop testing of a jet engine fuel control unit in flight conditions, Elsevier, Simul. Model. Pract. Theory 21 (2012) 6577

[14] A.S. Movaghar, A. Novinzadeh, Ideal Turbo Charger Modeling and Simulation Using bond graph Approach. in: ASME 2011 Turbo Expo: Turbine Technical Conference and Exposition, American Society of Mechanical Engineers, 2011, pp. 871–879

[15] M. Montazeri-Gh, S.A. Miran-F, Application of bond graph method in microjet engine cold start modeling to investigate the idea of injecting compressed air, in: Applied Mechanics and Materials, Trans Tech Publications, Vol. 799, 2015

[16] N.J. Krikelis, F. Papadakis. Gas turbine modelling using pseudo-bond graphs, Int. J. Syst. Sci. 19 (1988) 537–550

[17] A. Sanei, A.B. Novinzadeh, M. Habibi. Addition of momentum and kinetic energy effects in supersonic compressible flow using pseudo bond graph approach. Math. Comput. Model. Dyn. Syst. 20 (2014) 491–503
[18] N. Uddin, J.T. Gravdahl, Bond graph modeling of centrifugal compression systems. Simulation 91 (2015) 998–1013
[19] M. Montazeri-Gh, S.A. Miran-F, Application of bond graph approach in dynamic modelling of industrial gas turbine, Mech. Ind. 18 (2017) 410
[20] M. Montazeri-Gh, S.A. Miran-F, Modeling and simulation of a two-shaft gas turbine propulsion system containing a frictional plate–type clutch, Proc. Inst. Mech. Eng. Part M: J. Eng. Maritime Environ. (2018), DOI: 10.1177/1475090218765378
[21] S.A. Miran-F, M. Montazeri-Gh, Modeling and simulation of Jet Quad aerial robot, knowledge-based engineering and innovation (KBEI), in: 2017 IEEE 4th International Conference on. IEEE, 2017
[22] S. Camporeale, B. Fortunato, M. Mastrovito, A modular code for real time dynamic simulation of gas turbines in simulink, ASME J. Eng. Gas Turbines Power 128 (2006) 506–517
[23] R. Chacartegui, D. Sánchez, A. Muonoz, T. Sánchez, Real time simulation of medium size gas turbines, Energy Convers. Manag. 52 (2011) 713–724
[24] N.U. Rahman, J.F. Whidborne. Real-time transient three spool turbofan engine simulation: a hybrid approach. J. Eng. Gas Turbines Power 131 (2009) 051602
[25] "SGT-600 Industrial Gas Turbine," Siemens Industrial Turbomachinery, Duisburg, Germany, 2005, http://www.energy.siemens.com/ru/pool/hq/power-generation/gas-turbines/SGT-600/downloads/SGT-600_GT_PowerGen_EN.pdf
[26] D.C. Karnopp, D.L. Margolis, R.C. Rosenberg, System dynamics: modeling, simulation, and control of mechatronic systems, John Wiley and Sons, Hoboken, NJ, 2012
[27] J.F. Broenink, 20-sim software for hierarchical bond graph/block-diagram models. Simul. Pract. Theory 7 (1999) 481–492
[28] M. Montazeri-Gh, S. Abyaneh, Real-time simulation of a turbo-shaft engine's electronic control unit, Mech. Ind. 18 (2017) 503
[29] https://www.slideshare.net/AliRafiei2/gas-turbine-training-power-point-sample. Last check: 2017-08-19

Cite this article as: M. Montazeri-Gh, S.A. Miran Fashandi, S. Abyaneh, Real-time simulation test-bed for an industrial gas turbine engine's controller, Mechanics & Industry **19**, 311 (2018)